
PromptRR: Diffusion Models as Prompt Generators for Single Image Reflection Removal

Tao Wang¹ Wanglong Lu² Kaihao Zhang³ Wenhan Luo⁴ Tae-Kyun Kim⁵ Tong Lu¹
Hongdong Li⁶ Ming-Hsuan Yang^{7,8}

Abstract

Existing single image reflection removal (SIRR) methods using deep learning tend to miss key low-frequency (LF) and high-frequency (HF) differences in images, affecting their effectiveness in removing reflections. To address this problem, this paper proposes a novel prompt-guided reflection removal (PromptRR) framework that uses frequency information as new visual prompts for better reflection performance. Specifically, the proposed framework decouples the reflection removal process into the prompt generation and subsequent prompt-guided restoration. For the prompt generation, we first propose a prompt pre-training strategy to train a frequency prompt encoder that encodes the ground-truth image into LF and HF prompts. Then, we adopt diffusion models (DMs) as prompt generators to generate the LF and HF prompts estimated by the pre-trained frequency prompt encoder. For the prompt-guided restoration, we integrate specially generated prompts into the PromptFormer network, employing a novel Transformer-based prompt block to effectively steer the model toward enhanced reflection removal. The results on commonly used benchmarks show that our method outperforms state-of-the-art approaches. The codes and models are available at <https://github.com/TaoWangzj/PromptRR>.

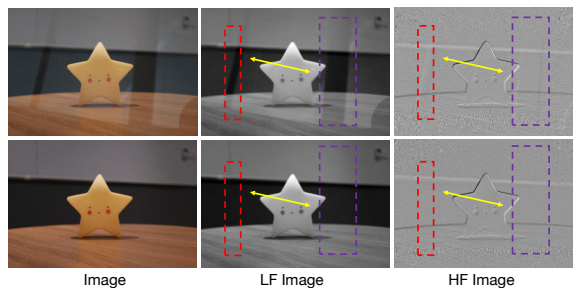


Figure 1. Illustration of the low-frequency and high-frequency images for both reflection and clear images. Both low- and high-frequency images of the reflected image exhibit distinct differences compared to those of the clear image. These differences tell if a region is reflection-dominated. This motivates us to develop a new SIRR method discerning and employing clear low and high frequencies as prompts to guide the deep model toward better reflection removal.

1. Introduction

Images taken through transparent surfaces, such as glass, usually contain undesirable specular reflections, significantly compromising the quality and visibility of the captured scenes. This degradation notably impacts the performance of computer vision applications like object detection and face recognition. Thus, single image reflection removal (SIRR) has received considerable interest in recent years.

Existing SIRR methods can be divided into two classes: early prior-based methods (Levin & Weiss, 2007; Levin et al., 2004; Shih et al., 2015; Wan et al., 2016; Yang et al., 2019) and recent deep learning-based methods (Fan et al., 2017; Yang et al., 2018; Zhang et al., 2018; Li et al., 2020; Song et al., 2023). Early prior-based methods mainly exploit image priors for reflection removal, such as gradient sparsity prior (Levin & Weiss, 2007), smoothness prior (Levin et al., 2004), and Gaussian mixture model prior (Shih et al., 2015). These priors are derived from the statistical characteristics of the reflection and background layers present in the given image. Although these prior-based methods are effective in certain situations consistent with specific physical mechanisms, they show limited robustness when dealing with complex and variable reflection scenarios. Thus, their reflec-

¹State Key Laboratory for Novel Software Technology, Nanjing University, Nanjing, China ²Memorial University of Newfoundland, St. John's, Canada ³Harbin Institute of Technology, Shenzhen, China ⁴Sun Yat-sen University, Shenzhen, China ⁵Imperial College London, London, UK & KAIST, Daejeon, South Korea ⁶Australian National University, Canberra, Australia ⁷University of California Merced, Merced, CA, USA ⁸Google Research.

tion performance degrades and their application is limited. Instead of using image priors, numerous methods develop different deep neural networks to estimate the background and reflection based on abundant labeled data. For example, several approaches (Fan et al., 2017; Yang et al., 2018) design an end-to-end convolutional neural network (CNN) to predict the clear image. Some methods adopt generative adversarial networks (Zhang et al., 2018), recurrent neural networks (Li et al., 2020), or transformer networks (Song et al., 2023) to build the network for reflection removal. In the case of reflection removal, the presence of reflections is primarily associated with the LF (low frequency) and HF (high frequency) components of images (Chung et al., 2009; Wan et al., 2018). As illustrated in Fig. 1, both the low- and high-frequency images of the reflected scene demonstrate significant deviations compared to those of the corresponding clear image counterparts. These differences tell if a region is reflection-dominated, providing valuable prompts for enhancing the network’s performance in removing reflections. However, it is rarely investigated in deep learning-based SIRR network design.

In this paper, we exploit the LF and HF information as a new visual prompt to guide the deep model for better reflection removal. To achieve this goal, there are mainly two important aspects in the model design: (1) *how to generate accurate LF and HF prompts*, and (2) *how to effectively utilize these prompts in the model to enhance reflection removal*. Some methods (Liu et al., 2018; Sajjadi et al., 2017) consider low and high frequencies of low-quality images in the model, which can improve the restoration performance. However, these methods are not specifically designed for SIRR and do not fully use the frequency information to help enhance image restoration. This limitation leads to their sub-optimal performance. To generate accurate LF and HF prompts and use these prompts for effective reflection removal, we decouple the reflection removal process into the prompt generation and subsequent prompt-guided restoration. For the prompt generation, we first propose a prompt pre-training strategy to train a frequency prompt encoder that can encode the ground-truth image into LF and HF prompts. Then, we train diffusion models (DMs) to generate LF and HF prompts estimated by the pre-trained frequency prompt encoder. Benefiting from the strong generation ability of DMs, we obtain accurate LF and HF prompts. For the prompt-guided restoration, we integrate the generated prompts into a tailored prompt-based transformer network that utilizes these prompts for effective reflection removal.

In particular, we propose a novel prompt-guided reflection removal method (PromptRR), which effectively utilizes frequency prompts to enhance the model’s capability to restore clear images. PromptRR consists of a frequency prompt encoder (FPE), two diffusion models (DMs), and a prompt transformer reflection network (PromptFormer). The pro-

cess of PromptRR contains prompt generation and prompt-guided restoration. For the prompt generation, PromptRR first adopts the strategy of prompt pre-training with FPE and PromptFormer, which aims to train the FPE so that it can encode accurate frequency prompts from the input ground truth image. Then, DMs are trained to generate the prompts encoded by the per-trained FPE. Finally, PromptRR utilizes the prompts generated by DMs to guide the PromptFormer during the reflection removal process. In PromptFormer, the key component is the proposed Transformer-based prompt block (TPB) which contains a prompt multi-head self-attention (PMSA) and a prompt feed-forward network (PFFN). In PMSA and PFFN, the core component is a prompt interaction and injection module. This module adaptively injects prompts into deep features, which guides the network to pay more attention to reflections for efficient reflection removal. Extensive evaluations against state-of-the-art methods on public real-world datasets demonstrate the superiority of PromptRR for SIRR.

The contributions of this paper are four-fold: (1) To the best of our knowledge, we make the first attempt to utilize frequency information as a new visual prompt in deep models to address the SIRR problem. (2) A novel SIRR framework PromptRR adopts diffusion models as prompt generators to generate high-quality low- and high-frequency prompts and uses these prompts for effective reflection removal. (3) A tailored PromptFormer is built by the proposed transformer-based prompt blocks, which help the model efficiently use frequency prompts for better reflection removal. (4) Extensive experiments on public real-world datasets demonstrate that PromptRR outperforms state-of-the-art methods.

2. Related Work

Single Image Reflection Removal. When capturing an image through transparent surfaces, reflection is an undesirable phenomenon. The reflection degradation can be modeled as (Schechner et al., 2000; Wei et al., 2019):

$$\mathbf{Q} = \mathbf{B} + \mathbf{R} * \mathbf{K}, \tag{1}$$

where \mathbf{Q} denotes the reflection-contaminated image, \mathbf{B} refers to the desired background layer, \mathbf{R} is the reflection content, $*$ represents a convolution operator, and \mathbf{K} is a Gaussian blur kernel. The above degradation model illustrates that SIRR is an ill-posed problem. SIRR (Fan et al., 2017; Wan et al., 2017) has received significant attention, and extensive SIRR methods have been proposed in the community. Generally, existing SIRR methods can be categorized into two groups: early prior-based methods and recent deep learning-based methods. Prior-based methods aim to extract the desired prior information from the reflection and background layers to help the model effectively achieve reflection removal. For example, sparsity prior (Levin &

Weiss, 2007), gradient sparsity prior (Levin et al., 2004), and Gaussian mixture model prior (Shih et al., 2015) are used for reflection removal. Unfortunately, these priors usually rely on certain physical models that do not fully encapsulate complex scenes, and thus the performance of prior-based methods degrades.

Recently, with the development of deep learning techniques, many deep learning-based SIRR methods have been proposed. In general, deep learning-based methods can be divided into single-stage and multi-stage methods. For single-stage SIRR methods, they typically involve the use of a single network for inference. For example, Zhang *et al.* (Zhang et al., 2018) incorporate the perceptual information into the conditional generative adversarial network (GAN). Wen *et al.* (WY19) (Wen et al., 2019) propose an alignment invariant loss that benefits the training of unaligned real-world images. Kim *et al.* (Kim et al., 2020) consider the spatial variability of reflections’ visual effects for reflection removal. Song *et al.* (Song et al., 2023) propose to use Transformers to build a robust network (RSIRR) for robust SIRR. Multi-stage SIRR methods adopt the multi-stage strategy in the network design to progressively refine the restored results. For instance, some methods employ two-stage (ZS21 (Zheng et al., 2021)) or three-stage (YG18 (Yang et al., 2018) and CL21 (Chang et al., 2021)) deep networks for reflection removal. Li *et al.* (LY20) (Li et al., 2020) introduce a multi-stage network that leverages long cascade networks with Long Short-Term Memory to achieve reflection removal. Hu and Guo (HG21) (Hu & Guo, 2021) incorporate interactions between two network branches, which can utilize information more effectively.

Diffusion Models. Recently, diffusion probabilistic models (DMs) (Sohl-Dickstein et al., 2015) have achieved remarkable success in various tasks such as image synthesis (Dhariwal & Nichol, 2021) and density estimation (Kingma et al., 2021). Compared with other generative models (GAN or VAE), DMs can effectively eliminate noise from a signal by employing parameterized Markov chains to optimize the lower variational bound on the likelihood function. Moreover, DMs exhibit desirable characteristics for sampling images, including distribution coverage, a stationary training objective, and easy scalability. As a result, more researchers have adopted DMs to tackle challenges in low-level vision, such as image super-resolution (Li et al., 2022; Saharia et al., 2023), image inpainting (Lugmayr et al., 2022), and image restoration (Saharia et al., 2022; Rombach et al., 2022). For example, the latent diffusion model (Rombach et al., 2022) is proposed to enhance restoration efficiency by implementing a diffusion process in the latent space. RePaint (Lugmayr et al., 2022) improves the denoising strategy to achieve higher visual quality for image inpainting. Palette (Saharia et al., 2022), through conditional diffusion models, advances the state of the art in four demanding

image-to-image translation tasks. These methods primarily concentrate on generating new content for individual pixels and exhibit a high degree of fidelity in their output generation. In contrast, our method conducts a diffusion process to predict frequency prompts to help the model achieve more effective reflection removal.

Prompt Learning. Prompt-based learning has garnered significant attention in the fields of natural language processing (NLP) and computer vision in recent years. Prompt-based methods involve conditioning pre-trained models with additional instructions to achieve specific tasks (Brown et al., 2020), and prompt plays a key role in downstream datasets (Zhou et al., 2022). Since using specific manual instruction sets as prompts requires domain expertise and is time-consuming (Zhou et al., 2022), some recent studies have started discussing the possibility of applying learnable prompts to achieve better performance on vision tasks (Zhou et al., 2022; Jia et al., 2022; Khattak et al., 2023), incremental learning (Wang et al., 2022b;c), and multitask learning (He et al., 2022; Wang et al., 2023c). However, most existing studies focus on high-level vision problems, and the potential of using prompt learning for SIRR remains unexplored. In our work, we propose a novel approach that combines prompt learning and diffusion models for SIRR. By using learnable prompts, we help models better remove reflections.

3. Methodology

3.1. Overall Pipeline

In this paper, we propose PromptRR, a frequency prompt learning-based framework for removing reflections. PromptRR effectively utilizes frequency prompts that have been learned to enhance the model’s capability to restore clear images. As shown in Fig. 2, PromptRR first adopts the strategy of prompt pre-training with a prompt encoder and a reflection removal network PromptFormer. The goal of the prompt pre-training is to train the prompt encoder to accurately extract the LF and HF prompts from input images. Then, the trained prompt encoder is utilized in the diffusion models to generate LF and HF prompts from the input degraded image. Finally, PromptRR utilizes these prompts to guide the PromptFormer during the reflection removal process. Next, we provide the details of the prompt pre-training and prompt generation and restoration stages of our method.

3.2. Prompt Pre-training

Recent advances in NLP-based text prompts have shown their potential in guiding models and improving prediction accuracy (Liu et al., 2023). However, applying text prompts directly to vision tasks, such as single reflection removal,

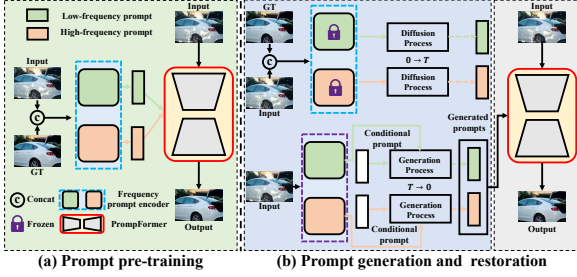


Figure 2. An overview of our PromptRR. It includes two main stages: (a) prompt pre-training stage and (b) prompt generation and restoration stage. Notably, we do not use the ground-truth image (GT) in the inference stage.

poses challenges due to the absence of accompanying text. Although previous methods (Herzig et al., 2022; Gan et al., 2023; Wang et al., 2023a) have explored text-free prompts like depth and segmentation prompts for vision tasks, these prompts may not be suitable for reflection removal. Therefore, our method introduces frequency prompts as a new visual prompt to guide the model for better reflection removal effectively. To achieve this goal, we propose a frequency prompt encoder (FPE) and a reflection removal network (PromptFormer) to conduct the prompt pre-training for the subsequent prompt generation by diffusion models. Next, we discuss the structures of FPE and PromptFormer and present the details of the prompt pre-training.

As shown in Fig. 3 (left), FPE mainly includes a wavelet transform (Huang et al., 2021; Zhou et al., 2023) and a dual-branch encoder. Within the dual-branch encoder, each branch mainly comprises residual blocks and linear layers. In FPE, the input images are fed to wavelet transform, resulting in LF and HF images. These images are then fed into the LF branch (depicted in green in Fig. 3) and the HF branch (depicted in light orange in Fig. 3) to generate LF and HF prompts, respectively. After that, PromptFormer adopts the generated prompts as guidance for better reflection removal. The overall structure of PromptFormer is shown in Fig. 3 (right). PromptFormer is a transformer-based reflection removal network, which contains a prompt-guided feature extractor, a prompt-guided reflection removal module, and a prompt-guided image reconstruction. The core block in PromptFormer is the transformer-based prompt block (TPB). We stack $N_{i \in [0,1,2,3]}$ TPBs to build the prompt-guided reflection removal module.

The transformer-based prompt block contains a prompt multi-head self-attention (PMSA) and a prompt feed-forward network (PFFN), which ensure the Transformers for better reflection removal by using the learned frequency prompts. The proposed TPB can be formulated as:

$$\begin{aligned} \mathbf{X}'_l &= \mathbf{X}_{l-1} + \text{PMSA}(\text{LN}(\mathbf{X}_{l-1}), \mathbf{P}), \\ \mathbf{X}_l &= \mathbf{X}'_l + \text{PFFN}(\text{LN}(\mathbf{X}'_l), \mathbf{P}), \end{aligned} \quad (2)$$

where \mathbf{X}_{l-1} and \mathbf{X}_l refer to the input and output features of the l^{th} TPB, and \mathbf{P} denotes LF or HF prompt.

Prompt Multi-head Self-attention. Existing Transformers (Zamir et al., 2022; Wang et al., 2022a; Song et al., 2023) typically extract query (Q), key (K), and value (V) from the input feature to perform multi-head self-attention. However, these Transformers may not be sufficiently effective in representing features without explicit visual cues. To overcome this challenge, we develop PMSA in the Transformers, aiming to enhance the network’s focus on extra visual prompts and thus improve its performance for reflection removal. Specifically, we propose a prompt interaction and injection module (PIIM), refining the input feature using prompts before generating Q , K , and V . The structure of PIIM is shown in Fig. 4 and consists of two steps: prompt interaction and prompt injection. For the prompt interaction step, we first use adaptive average pooling followed by two linear layers to transform input feature \mathbf{X}_{l-1} into $\hat{\mathbf{X}}_{l-1}$ with the same shape with the prompt \mathbf{P} . Then, we conduct a cross-attention interaction between \mathbf{P} and $\hat{\mathbf{X}}_{l-1}$ in the spatial dimension. The cross-attention interaction process is shown as:

$$\begin{aligned} Q &= W^Q \hat{\mathbf{X}}_{l-1}, K_p = W^K \mathbf{P}, V = W^V \hat{\mathbf{X}}_{l-1}, \\ \mathbf{P}' &= \text{Adap}(\text{Softmax}\left(\frac{QK^T}{\alpha}\right) V), \end{aligned} \quad (3)$$

where W^Q , W^K , and W^V denote the projection matrices of the query, key, and value. α is an optional temperature factor and Adap is the adaptive average pooling operation. Then, \mathbf{P}' is further refined by \mathbf{P} using two learnable fusion parameters (Wei et al., 2022; Huang & Belongie, 2017) shown as:

$$\mathbf{P}_r = \frac{\mathbf{P}' - \mu}{\sigma} \odot (1 + \gamma) + \beta, \quad (4)$$

where \mathbf{P}_r is the refined prompt, \odot is element-wise multiplication, μ and σ are the mean and standard deviation of \mathbf{P}' respectively. γ and β are produced by $f_\gamma(\mathbf{P})$ and $f_\beta(\mathbf{P})$ that are implemented with two simple linear layers with one intermediate layernorm and leaky relu layer.

For the prompt injection step, the refined prompt \mathbf{P}_r is injected into \mathbf{X}_{l-1} to derive the prompt modulation feature \mathbf{X}'_{l-1} as:

$$\mathbf{X}'_{l-1} = W_1 \mathbf{P}_r \odot \mathbf{X}_{l-1} + W_2 \mathbf{P}_r, \quad (5)$$

where W_1 and W_2 denote the linear layer. After that, we apply a 1×1 convolution, followed by a 3×3 depth-wise convolution, to generate the query, key, and value from the modulation feature, respectively. Additionally, we perform self-attention across channels instead of the spatial dimension, aiming to reduce the time and memory complexity. This design choice is inspired by recent works (Zamir et al., 2022; Wang et al., 2023b; Xia et al., 2023).

Prompt Feed-forward Network. To make full use of the frequency prompt information in the network, we also introduce our plug-and-play PIIM into the recent feed-forward

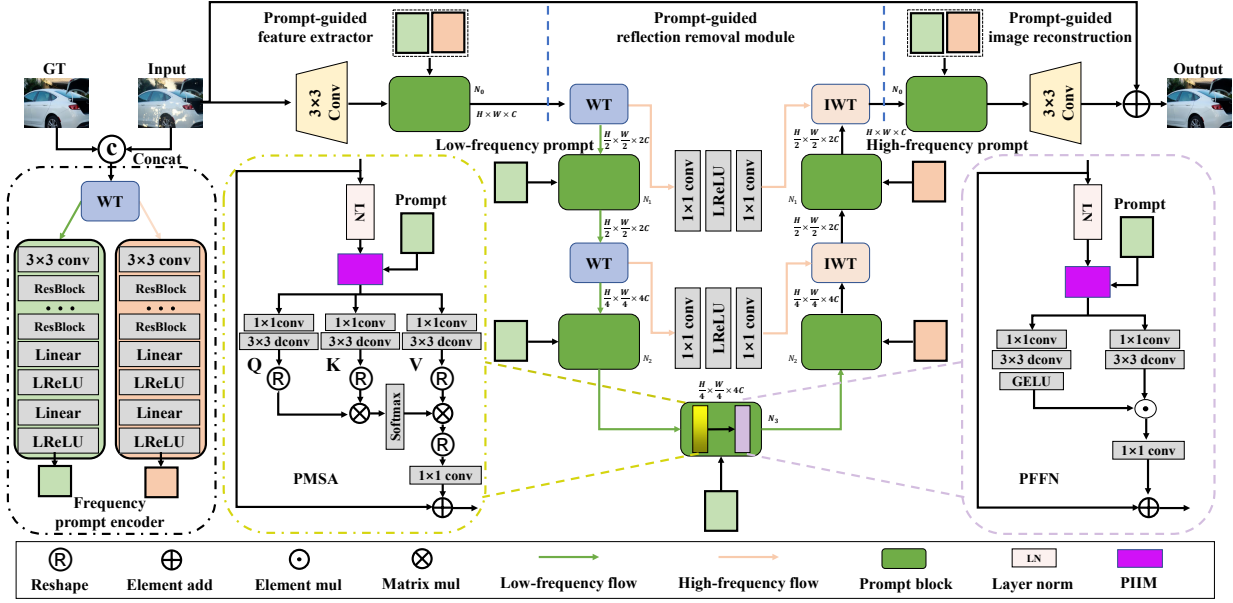


Figure 3. The overview of FPE and PromptFormer for the prompt pre-training. FPE includes a wavelet transform and a dual-branch encoder. PromptFormer is mainly built by a transformer-based prompt block consisting of the prompt multi-head self-attention (PMSA) and the prompt feed-forward network (PFFN). WT and IWT refer to the wavelet transform and inverse wavelet transform respectively.

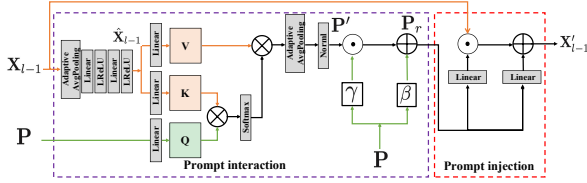


Figure 4. Architecture of the prompt interaction and injection module (PIIM). PIIM contains two stages: Prompt interaction and injection. In the feature extractor and image reconstruction stages of PromptFormer, we only use prompt injection in TPBs.

network (Zamir et al., 2022; Xia et al., 2023) to build our PFFN, which is shown in Fig. 3 (right). More details are provided in the supplemental material.

For prompt pre-training, we train FPE and PromptFormer together using the \mathcal{L}_1 loss:

$$\mathcal{L}_1 = \|I_r - I_{gt}\|_1, \quad (6)$$

where I_r is the restored result of PromptFormer and I_{gt} is the ground-truth image. With this prompt pre-training, FPE can produce LF and HF prompts accurately for subsequent prompt generation by diffusion models.

3.3. Prompt Generation and Restoration

To generate more accurate prompts for better reflection removal, we present a dual-diffusion model as a prompt generator by taking advantage of the powerful generative abilities of diffusion models. As shown in Fig. 2, our prompt generator consists of a low-frequency generation diffusion model

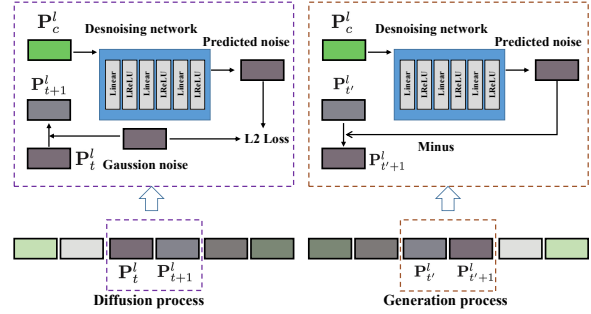


Figure 5. The overall structure of the prompt generation where we use the low-frequency generation diffusion model as an example.

and a high-frequency generation diffusion model. These two diffusion models share the same architecture, where the denoise network is implemented by several linear layers with leaky relu (Huang & Belongie, 2017; Xia et al., 2023). The diffusion model contains two processes, *i.e.*, the diffusion process and the generation process. For ease of illustration, we use the low-frequency generation diffusion as an example of these two processes in the following.

Diffusion Process. During the diffusion process, we first adopt the pre-trained FPE to produce initial LF and HF prompt vectors (*i.e.*, \mathbf{P}^l and \mathbf{P}^h). Then, continuously adding Gaussian noise to the initial prompt vectors, the characteristics of the prompt vectors will gradually disappear, and the prompt eventually becomes standard Gaussian noise. Specifically, as illustrated in Fig. 5, at the diffusion step

Table 1. Comparison of quantitative results on commonly used real-world datasets in terms of PSNR and SSIM. **Bold** and underline indicate the best and second-best results.

Methods	Nature (Li et al., 2020)		SIR ² (Wan et al., 2017)								Real (Zhang et al., 2018)	
			Postcard		SolidObject		WildScene		Average			
	PSNR	SSIM	PSNR	SSIM	PSNR	SSIM	PSNR	SSIM	PSNR	SSIM	PSNR	SSIM
WY19 (Wei et al., 2019)	19.54	0.7390	17.02	0.7528	22.28	0.8072	22.07	0.8196	20.27	0.7895	21.82	0.7599
WT19 (Wen et al., 2019)	10.45	0.1593	7.63	0.2871	10.81	0.2359	11.16	0.1945	9.70	0.2463	11.66	0.0928
LY20 (Li et al., 2020)	19.41	0.7557	17.58	0.7807	23.34	0.8480	23.27	0.8855	21.18	0.8308	22.65	0.7785
ZS21 (Zheng et al., 2021)	18.07	0.7496	16.11	0.7507	19.65	0.7538	20.02	0.8228	18.41	0.7672	19.15	0.6659
CL21 (Chang et al., 2021)	20.02	0.7786	18.89	0.7861	23.42	0.8327	24.02	0.8964	21.86	0.8287	22.12	0.7721
HG21 (Hu & Guo, 2021)	20.44	<u>0.7901</u>	18.65	0.8076	24.05	0.8566	23.86	0.8897	22.00	0.8453	22.11	0.7751
Uformer (Wang et al., 2022a)	19.94	0.7826	19.28	0.7822	22.61	0.8226	22.91	0.8923	21.43	0.8222	20.04	0.7267
Restormer (Zamir et al., 2022)	20.71	0.7794	17.80	0.7848	24.07	0.8570	24.04	0.8490	21.73	0.8388	20.38	0.7315
RSIRR (Song et al., 2023)	<u>20.97</u>	0.7864	<u>19.65</u>	<u>0.8230</u>	24.71	0.8700	<u>24.70</u>	<u>0.8976</u>	<u>22.82</u>	<u>0.8583</u>	<u>23.61</u>	<u>0.7912</u>
PromptRR (Ours)	21.00	0.8142	23.03	0.8653	<u>24.17</u>	0.8587	26.43	0.9300	24.22	0.8761	24.11	0.8126

t , the next noisy prompt vector \mathbf{P}_{t+1}^l can be obtained by $\mathbf{P}_{t+1}^l = \mathbf{P}_t^l + \epsilon$, where ϵ is the Gaussian noise. After that, the next noisy prompt and the proposed conditions are fed into the denoise network ϵ_θ to estimate the distribution of the noise, which is optimized by the squared error loss:

$$\mathcal{L}_{diff}^l = \|\epsilon - \epsilon_\theta(\mathbf{P}_c^l, \mathbf{P}_{t+1}^l, t)\|^2, \quad (7)$$

where \mathbf{P}_c^l represents the conditional prompt that is extracted from the reflection-contaminated input by FPE. Specifically, given the diffusion step, \mathcal{L}_{diff}^l can be directly calculated by the original prompt rather than the intermediate status.

Generation Process. In the generation process, the prompt vector is finally generated by gradually denoising the random initial Gaussian noise vector under the conditional prompt from the FPE. Specifically, at the generation step t' , the denoising prompt vector $\mathbf{P}_{t'}^l$ and the conditional prompt \mathbf{P}_c^l are fed into the denoise network to predict the noise.

Then, the next denoising prompt vector $\mathbf{P}_{t'+1}^l$ is obtained by subtracting the predicted noise from the current denoising prompt vector. This process can be formulated as:

$$\mathbf{P}_{t'+1}^l = \mathbf{P}_{t'}^l - \epsilon_\theta(\mathbf{P}_c^l, \mathbf{P}_{t'}^l, t'). \quad (8)$$

After the dual-diffusion model generates the frequency prompts $\hat{\mathbf{P}}_{T \rightarrow 0}^l$ and $\hat{\mathbf{P}}_{T \rightarrow 0}^h$, our PromptFormer incorporates them as guidance for better reflection removal. Specifically, in the stage of prompt generation and restoration, we first train this diffusion model individually in some iterations and then train PromptFormer and the diffusion model together. The joint training loss \mathcal{L} is:

$$\mathcal{L} = \mathcal{L}_{diff}^l + \mathcal{L}_{diff}^h + \mathcal{L}_1, \quad (9)$$

where \mathcal{L}_{diff}^l and \mathcal{L}_{diff}^h denote the diffusion losses of low-frequency diffusion and the high-frequency diffusion models. \mathcal{L}_1 is the pixel-wise loss from PromptFormer.

For inference, given the input image, our model first uses diffusion models to generate the LF and HF prompts, and then the generated prompts and the input image are fed into the PromptFormer to recover the final clear image.

4. Experiments

4.1. Experimental settings

Datasets and Metrics. We conduct experiments on popular benchmarks. Following previous works (Hu & Guo, 2021; Song et al., 2023), we train our networks on a dataset consisting of a combination of synthetic and real-world data. For the synthetic training data, we adopt the PASCAL VOC dataset (Everingham et al., 2010) to synthesize 7,643 images using the data-generation method described in (Fan et al., 2017). For the real-world data, we adopt 90 real-world training images from (Zhang et al., 2018). In the testing phase, we evaluate models on three commonly used real-world datasets, Nature (Li et al., 2020), SIR² (Wan et al., 2017), and Real dataset (Zhang et al., 2018). The SIR² dataset comprises three subsets, namely *PostCard*, *SolidObject*, and *WildScene*. In addition, PSNR (Huynh-Thu & Ghanbari, 2008) and SSIM (Wang et al., 2004) are used as the metrics for performance evaluation.

Comparison SIRR Methods. We compare the proposed PromptRR with six CNN-based SIRR methods (WY19 (Wei et al., 2019), WT19 (Wen et al., 2019), LY20 (Li et al., 2020), ZS21 (Zheng et al., 2021), CL21 (Chang et al., 2021), HG21 (Hu & Guo, 2021) and one recent Transformer-based SIRR method (RSIRR (Song et al., 2023)), and two general Transformer-based image restoration methods (Uformer (Wang et al., 2022a) and Restormer (Zamir et al., 2022)).

Training Details. Our PromptRR framework contains two stages: prompt pre-training, and prompt generation and restoration. In PromptFormer, N_0, N_1, N_2, N_3 are set to 4, 6, 6, 8, and the number of attention heads is set to 1, 2, 4, 8. The initial channel C is 48. Specifically, in the prompt pre-training stage, we employ the AdamW optimizer to train our FPE and PromptFormer models. The training is performed with a batch size of 8 and a patch size of 128 for a total of 200,000 iterations. The learning rate is set to 1×10^{-4} . For the prompt generation and restoration stage, we utilize the Adam optimizer with a batch size of 8 and a patch size

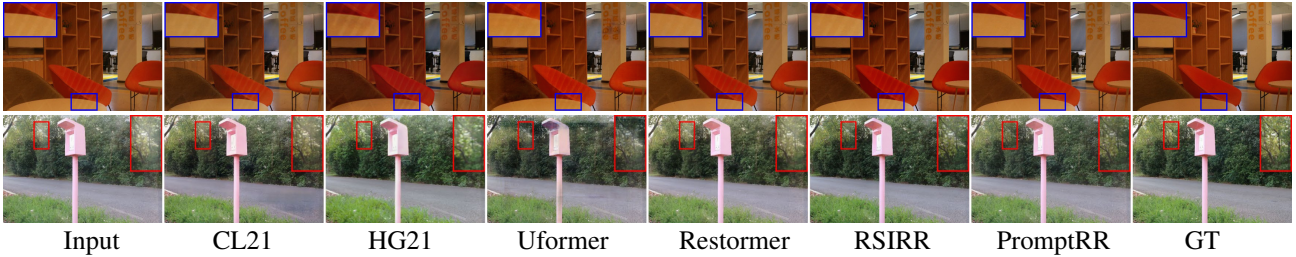


Figure 6. Visual comparison on *Nature* dataset. Compared with other methods, our PromptRR effectively removes reflections while preserving the fine details in the restored images.

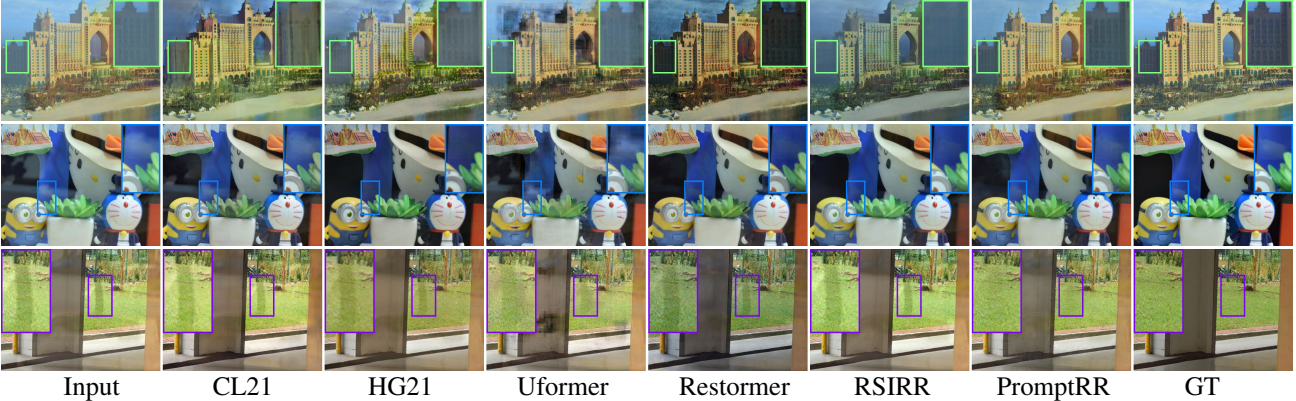


Figure 7. Visual comparison on *SIR²* dataset. The images are from three subsets: *Postcard* (1st row), *SolidObject* (2nd row), and *WildScene* (3rd row). In contrast, our PromptRR removes more undesired reflections and produces clearer images (see bounding boxes).

of 128. In the initial phase, the dual-diffusion model is trained for 20,000 iterations. Subsequently, we jointly train the dual-diffusion model and PromptFormer for a total of 280,000 iterations. The learning rate is set to 1×10^{-4} . For the diffusion modes, the total timestep T is set to 4. More details are provided in the supplementary material.

4.2. Comparisons Results

Quantitative Results. Table 1 presents the quantitative comparisons of our method with the SOTA SIRR methods on commonly used real-world datasets. Recent image restoration methods Restormer (Zamir et al., 2022) and Uformer (Wang et al., 2022a) adopt an end-to-end network to achieve image restoration. However, they do not consider explicitly reflection-conditional guidance to help the process of restoration. Thus, these methods do not effectively remove reflection. Although RSIRR (Song et al., 2023) utilizes cross-scale attention, multi-scale, and adversarial mechanisms to address SIRR, its performance is still unsatisfactory. In contrast, our PromptRR can explore frequency prompts to guide the process of reflection removal. As shown in Table 1, our PromptRR achieves the best performance in terms of PSNR and SSIM on all real-world datasets, where the average PSNR value is 1.4 dB higher than the second-place method RSIRR (Song et al., 2023) on *SIR²* dataset.

Qualitative Results. We also show visual comparisons

Table 2. Effectiveness of the proposed PIIM.

Models	w/o Interaction	w/o PIIM	w/ PIIM (Ours)
PSNR/SSIM	23.51/0.8011	20.25/0.7247	24.04/0.8103

of the reflection removal results obtained from five SOTA models and our PromptRR. Specifically, as demonstrated in Fig. 6, Fig. 7, and Fig. 8, we present visual comparisons on the employed datasets. Our method effectively removes reflections, yielding images that closely resemble the ground truth. In Fig. 6, though the compared methods can conduct restoration well, striped shadow effects still exist in the region highlighted by the blue boxes in the first row. In comparison, our method shows a clear table surface. Fig. 7 (the third-row purple boxes) illustrates the failure of compared methods to eliminate shadow effects, in contrast to our approach, which is capable of removing reflections to produce more pleasing glasses. In Fig. 8, under severe degradation, most methods struggle to clarify toy structures and textures, while PromptRR produces the restored images with better structural fidelity. As a result, our method shows its superiority compared to other existing methods. More qualitative results can be found in our supplemental material.

4.3. Ablation Study

To gain a comprehensive understanding of how our method tackles the issue of SIRR and to show the impact of its primary components, we conduct a comprehensive analysis

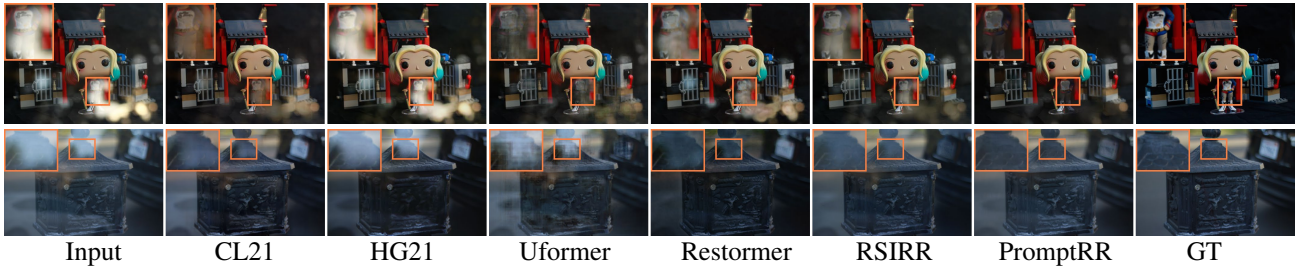


Figure 8. Visual comparison on *Real* dataset. The reflection results of comparison methods still contain significant reflection effects. Our PromptRR removes the reflection areas more accurately and thoroughly.

Table 3. Effectiveness of the prompt for reflection removal.

Models	MSA	FFN	PMSA	PFFN	PSNR/SSIM
(a)	✓	✓			20.25/0.7247
(b)	✓			✓	23.29/0.8010
(c)		✓	✓		22.48/0.7973
Ours			✓	✓	24.04/0.8103

Table 4. Ablation study on prompt generation using DMs.

PromptRR	w/o DMs	w/ DMs
PSNR/SSIM	19.95/0.7328	24.04/0.8103

of the proposed method. To ensure fair comparisons in the ablation studies, we train all model variants on the training set for 100,000 iterations only. We evaluate the models on *Real* testing set in terms of PSNR and SSIM.

Effectiveness of PIIM. To verify whether our PIIM facilitates reflection removal, we conduct ablation studies by setting two other variants: (1) removing the prompt interaction stage in PIIM from the model, and (2) removing all PIIM from the model, respectively. Table 2 presents that our full model with the proposed PIIM exhibits superior performance compared to other models, where the PSNR and SSIM values surpass that of the model without PIIM by 3.79 dB and 0.0856. Moreover, we observe that the model incorporating the prompt interaction stage in PIIM achieves higher PSNR and SSIM values. Specifically, the PSNR value is 0.53 dB higher compared to the model without the prompt interaction stage in PIIM. This suggests that using the prompt interaction in PIIM aids in refining and reinforcing prompts for better reflection removal.

Effectiveness of Prompt. In our method, we employ our transformer-based prompt block as the basic unit for constructing our PromptFormer. Within the prompt block, we introduce the frequency prompt into the plain multi-head self-attention (MAS) and plain feed-forward network (FFN) (Zamir et al., 2022) to construct the core modules PMSA and PFFN. To better demonstrate the effectiveness of the prompt used in PMSA and PFFN, we conduct an ablation study that considers the position of the prompt used in the prompt block. As shown in Table 3, we build three

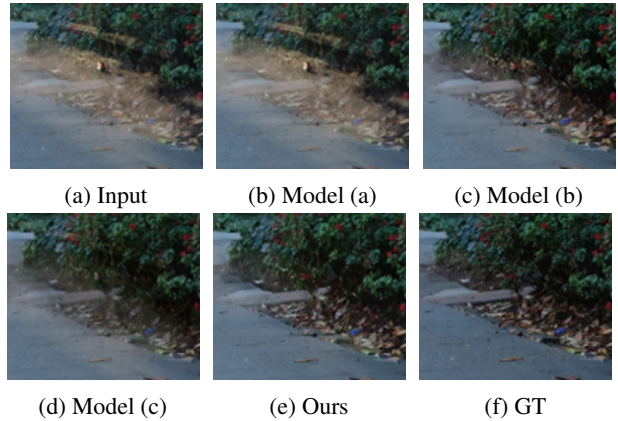


Figure 9. Visual comparison between our method and variants.

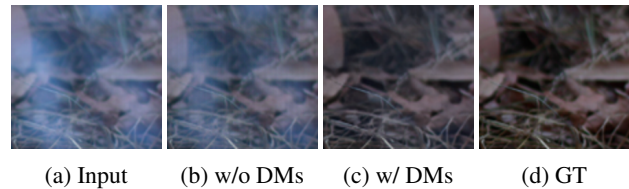


Figure 10. Ablation comparison for DMs for prompt generation.

baselines with different positions of the prompt used within the prompt block: (a) without using any frequency prompt in both MSA and FFN, (b) using the frequency prompt in FFN, and (c) using the frequency prompt in MSA. The quantitative and qualitative results are shown in Table 3 and Fig. 9. When using the prompt in MSA (c) or FFN (b), the models’ performance is improved. Compared to other baselines, our model yields the best performance after introducing the prompt into MSA and FFN, which validates the effectiveness of the prompt. Fig. 9 further shows that using the prompts as guidance in the model can facilitate reflection removal.

Effectiveness of DMs for Prompt Generation. We further demonstrate the effectiveness of DMs for prompt generation. In Table 4, “w/o DMs” means that we use a CNN network to replace the DMs for prompt generation in our PromptPR. “DMs” refers to our PromptRR using diffusion models to generate prompts for guiding reflection removal. The results

are listed in Table. 4 and Fig. 10. It shows that using DMs for prompt generation achieves the best performance of reflection removal in PSNR and SSIM and the best visual effects. Compared with the model without DMs as prompt generators, the improvement gains in PSNR and SSIM are 4.09 dB and 0.0775 respectively. From Fig. 10, we observe that using DMs as the prompt generator to generate prompts, our PromptRR achieves the closest visual results to the ground truth. In contrast, the model w/o DMs fails to remove reflection in the image. Thus, the results show that the DMs have powerful abilities for high-quality prompt generation.

5. Conclusion

In this paper, we propose a novel prompt-guided reflection removal framework (PromptRR) that adopts DMs as frequency prompt generators and uses the prompt for effective reflection removal. We decouple the reflection removal process into the prompt generation and subsequent prompt-guided restoration. To generate high-quality frequency prompts, we adopt a prompt pre-training strategy and train DMs to generate prompts. After that, we view the trained DMs as frequency prompt generators to first generate prompts and then embed the prompts into the prompt transformer network (PromptFormer) for effective reflection removal. Experimental results show that our PromptRR is superior to state-of-the-art methods.

References

- Brown, T., Mann, B., Ryder, N., Subbiah, M., Kaplan, J. D., Dhariwal, P., Neelakantan, A., Shyam, P., Sastry, G., Askell, A., et al. Language models are few-shot learners. In *NeurIPS*, pp. 1877–1901, 2020.
- Chang, Y.-C., Lu, C.-N., Cheng, C.-C., and Chiu, W.-C. Single image reflection removal with edge guidance, reflection classifier, and recurrent decomposition. In *WACV*, pp. 2032–2041, 2021.
- Chung, Y.-C., Chang, S.-L., Wang, J.-M., and Chen, S.-W. Interference reflection separation from a single image. In *WACV*, pp. 1–6, 2009.
- Dhariwal, P. and Nichol, A. Q. Diffusion models beat GANs on image synthesis. In *NeurIPS*, pp. 8780–8794, 2021.
- Everingham, M., Van Gool, L., Williams, C. K. I., Winn, J., and Zisserman, A. The pascal visual object classes (voc) challenge. *IJCV*, 88(2):303–338, 2010.
- Fan, Q., Yang, J., Hua, G., Chen, B., and Wipf, D. A generic deep architecture for single image reflection removal and image smoothing. In *ICCV*, pp. 3238–3247, 2017.
- Gan, Y., Bai, Y., Lou, Y., Ma, X., Zhang, R., Shi, N., and Luo, L. Decorate the newcomers: Visual domain prompt for continual test time adaptation. In *AAAI*, pp. 7595–7603, 2023.
- He, Y., Zheng, S., Tay, Y., Gupta, J., Du, Y., Aribandi, V., Zhao, Z., Li, Y., Chen, Z., Metzler, D., et al. Hyperprompt: Prompt-based task-conditioning of transformers. In *ICML*, pp. 8678–8690, 2022.
- Herzig, R., Abramovich, O., Ben-Avraham, E., Arbel, A., Karlinsky, L., Shamir, A., Darrell, T., and Globerson, A. Promptonomyvit: Multi-task prompt learning improves video transformers using synthetic scene data. *arXiv preprint arXiv:2212.04821*, 2022.
- Hu, Q. and Guo, X. Trash or treasure? an interactive dual-stream strategy for single image reflection separation. In *NeurIPS*, pp. 24683–24694, 2021.
- Huang, H., Yu, A., Chai, Z., He, R., and Tan, T. Selective wavelet attention learning for single image deraining. *IJCV*, 129:1282–1300, 2021.
- Huang, X. and Belongie, S. Arbitrary style transfer in real-time with adaptive instance normalization. In *ICCV*, pp. 1501–1510, 2017.
- Huynh-Thu, Q. and Ghanbari, M. Scope of validity of psnr in image/video quality assessment. *Electronics Letters*, 44(13): 800–801, 2008.
- Jia, M., Tang, L., Chen, B.-C., Cardie, C., Belongie, S., Hariharan, B., and Lim, S.-N. Visual prompt tuning. In *ECCV*, pp. 709–727, 2022.
- Khattak, M. U., Rasheed, H., Maaz, M., Khan, S., and Khan, F. S. Maple: Multi-modal prompt learning. In *CVPR*, pp. 19113–19122, 2023.
- Kim, S., Huo, Y., and Yoon, S.-E. Single image reflection removal with physically-based training images. In *CVPR*, pp. 5163–5172, 2020.
- Kingma, D., Salimans, T., Poole, B., and Ho, J. Variational diffusion models. In *NeurIPS*, pp. 21696–21707, 2021.
- Levin, A. and Weiss, Y. User assisted separation of reflections from a single image using a sparsity prior. *IEEE TPAMI*, 29(9): 1647–1654, 2007.
- Levin, A., Zomet, A., and Weiss, Y. Separating reflections from a single image using local features. In *CVPR*, pp. 306–313, 2004.
- Li, C., Yang, Y., He, K., Lin, S., and Hopcroft, J. E. Single image reflection removal through cascaded refinement. In *CVPR*, pp. 3565–3574, 2020.
- Li, H., Yang, Y., Chang, M., Chen, S., Feng, H., Xu, Z., Li, Q., and Chen, Y. Srdiff: Single image super-resolution with diffusion probabilistic models. *Neurocomputing*, 479:47–59, 2022.
- Liu, P., Zhang, H., Zhang, K., Lin, L., and Zuo, W. Multi-level wavelet-cnn for image restoration. In *CVPR*, pp. 773–782, 2018.
- Liu, P., Yuan, W., Fu, J., Jiang, Z., Hayashi, H., and Neubig, G. Pre-train, prompt, and predict: A systematic survey of prompting methods in natural language processing. *ACM Computing Surveys*, 55(9):1–35, 2023.
- Lugmayr, A., Danelljan, M., Romero, A., Yu, F., Timofte, R., and Van Gool, L. Repaint: Inpainting using denoising diffusion probabilistic models. In *CVPR*, pp. 11461–11471, 2022.

- Rombach, R., Blattmann, A., Lorenz, D., Esser, P., and Ommer, B. High-resolution image synthesis with latent diffusion models. In *CVPR*, pp. 10684–10695, 2022.
- Saharia, C., Chan, W., Chang, H., Lee, C., Ho, J., Salimans, T., Fleet, D., and Norouzi, M. Palette: Image-to-image diffusion models. In *ACM SIGGRAPH*, pp. 1–10, 2022.
- Saharia, C., Ho, J., Chan, W., Salimans, T., Fleet, D. J., and Norouzi, M. Image super-resolution via iterative refinement. *IEEE TPAMI*, 45(4):4713–4726, 2023.
- Sajjadi, M. S. M., Schölkopf, B., and Hirsch, M. Enhancenet: Single image super-resolution through automated texture synthesis. In *ICCV*, pp. 4501–4510, 2017.
- Schechner, Y. Y., Kiryati, N., and Basri, R. Separation of transparent layers using focus. *IJCV*, 39:25–39, 2000.
- Shih, Y., Krishnan, D., Durand, F., and Freeman, W. T. Reflection removal using ghosting cues. In *CVPR*, pp. 3193–3201, 2015.
- Sohl-Dickstein, J., Weiss, E., Maheswaranathan, N., and Ganguli, S. Deep unsupervised learning using nonequilibrium thermodynamics. In *ICML*, pp. 2256–2265, 2015.
- Song, Z., Zhang, Z., Zhang, K., Luo, W., Fan, Z., Ren, W., and Lu, J. Robust single image reflection removal against adversarial attacks. In *CVPR*, pp. 24688–24698, 2023.
- Wan, R., Shi, B., Hwee, T. A., and Kot, A. C. Depth of field guided reflection removal. In *ICIP*, pp. 21–25, 2016.
- Wan, R., Shi, B., Duan, L.-Y., Tan, A.-H., and Kot, A. C. Benchmarking single-image reflection removal algorithms. In *ICCV*, pp. 3942–3950, 2017.
- Wan, R., Shi, B., Duan, L.-Y., Tan, A.-H., Gao, W., and Kot, A. C. Region-aware reflection removal with unified content and gradient priors. *IEEE TIP*, 27(6):2927–2941, 2018.
- Wang, C., Pan, J., Lin, W., Dong, J., and Wu, X.-M. Selfpromer: Self-prompt dehazing transformers with depth-consistency. *arXiv preprint arXiv:2303.07033*, 2023a.
- Wang, T., Zhang, K., Shen, T., Luo, W., Stenger, B., and Lu, T. Ultra-high-definition low-light image enhancement: A benchmark and transformer-based method. In *AAAI*, pp. 2654–2662, 2023b.
- Wang, Z., Bovik, A. C., Sheikh, H. R., and Simoncelli, E. P. Image quality assessment: from error visibility to structural similarity. *IEEE TIP*, 13(4):600–612, 2004.
- Wang, Z., Cun, X., Bao, J., Zhou, W., Liu, J., and Li, H. Uformer: A general u-shaped transformer for image restoration. In *CVPR*, pp. 17683–17693, 2022a.
- Wang, Z., Zhang, Z., Ebrahimi, S., Sun, R., Zhang, H., Lee, C.-Y., Ren, X., Su, G., Perot, V., Dy, J., et al. Dualprompt: Complementary prompting for rehearsal-free continual learning. In *ECCV*, pp. 631–648, 2022b.
- Wang, Z., Zhang, Z., Lee, C.-Y., Zhang, H., Sun, R., Ren, X., Su, G., Perot, V., Dy, J., and Pfister, T. Learning to prompt for continual learning. In *CVPR*, pp. 139–149, 2022c.
- Wang, Z., Panda, R., Karlinsky, L., Feris, R., Sun, H., and Kim, Y. Multitask prompt tuning enables parameter-efficient transfer learning. *arXiv preprint arXiv:2303.02861*, 2023c.
- Wei, K., Yang, J., Fu, Y., Wipf, D., and Huang, H. Single image reflection removal exploiting misaligned training data and network enhancements. In *CVPR*, pp. 8178–8187, 2019.
- Wei, T., Chen, D., Zhou, W., Liao, J., Tan, Z., Yuan, L., Zhang, W., and Yu, N. Hairclip: Design your hair by text and reference image. In *CVPR*, pp. 18072–18081, 2022.
- Wen, Q., Tan, Y., Qin, J., Liu, W., Han, G., and He, S. Single image reflection removal beyond linearity. In *CVPR*, pp. 3771–3779, 2019.
- Xia, B., Zhang, Y., Wang, S., Wang, Y., Wu, X., Tian, Y., Yang, W., and Van Gool, L. Diffir: Efficient diffusion model for image restoration. *arXiv preprint arXiv:2303.09472*, 2023.
- Yang, J., Gong, D., Liu, L., and Shi, Q. Seeing deeply and bidirectionally: A deep learning approach for single image reflection removal. In *ECCV*, pp. 654–669, 2018.
- Yang, Y., Ma, W., Zheng, Y., Cai, J.-F., and Xu, W. Fast single image reflection suppression via convex optimization. In *CVPR*, pp. 8141–8149, 2019.
- Zamir, S. W., Arora, A., Khan, S., Hayat, M., Khan, F. S., and Yang, M.-H. Restormer: Efficient transformer for high-resolution image restoration. In *CVPR*, pp. 5728–5739, 2022.
- Zhang, X., Ng, R., and Chen, Q. Single image reflection separation with perceptual losses. In *CVPR*, pp. 4786–4794, 2018.
- Zheng, Q., Shi, B., Chen, J., Jiang, X., Duan, L.-Y., and Kot, A. C. Single image reflection removal with absorption effect. In *CVPR*, pp. 13395–13404, 2021.
- Zhou, K., Yang, J., Loy, C. C., and Liu, Z. Learning to prompt for vision-language models. *IJCV*, 130(9):2337–2348, 2022.
- Zhou, Y., Huang, J., Wang, C., Song, L., and Yang, G. Xnet: Wavelet-based low and high frequency fusion networks for fully- and semi-supervised semantic segmentation of biomedical images. In *ICCV*, pp. 21085–21096, 2023.